Explainable Neuro-Symbolic Learning for Mohs Hardness Prediction in Mining and Mineral Processing

Mohammed I. Thanoon[1], Sami F. Karali[2], Mohamed H. Helal[3]*,
Ahlem Fatnassi[4], Majed Nawas[5], Monir Abdullah[6], Asma A. Alhashmi[7], Abdulbasit A. Darem[8]
Computing Department-College of Engineering and Computing at Al-Lith, Umm Al-Qura University, Makkah, Saudi Arabia[1, 2]
Center for Scientific Research and Entrepreneurship, Northern Border University, 73213, Arar, Saudi Arabia[3, 8]
Department of Computer Science-College of Science, Northern Border University, Arar 73213, Saudi Arabia[4, 5, 7]
Department of Computer Science and Artificial Intelligence-College of Computing and Information Technology,
University of Bisha, Bisha 61922, Saudi Arabia[6]

***Abstract*—Predicting Mohs hardness from mineralogical information is still a challenging task because of the complex and nonlinear relationship between mineral composition and hardness properties. Traditional machine learning (ML) and deep learning (DL) strategies have been used to address this study, exploiting mineralogical attributes for prediction. Conversely, these techniques are frequently highly dependent on large labeled datasets, struggle to generalize over distinct mineral categories, and face challenges in extracting subtle physicochemical interactions and delivering interpretable predictions. This study presents an Explainable Deep Representation Learning Framework based on Mohs Hardness Prediction (XDRL-MHP). The primary objective of this work is to predict Mohs hardness using mineralogical properties by modeling mineral composition and structural characteristics. The proposed model employs mRMR for feature selection to identify the most informative physicochemical attributes. A physicochemical representation constructed using atomic interaction mapping, periodic table relationship encoding, chemical affinity representation, and molecular dependency construction to capture complex mineral relationships. Besides, a neuro-symbolic hybrid architecture is designed by integrating a capsule network for hierarchical mineral pattern learning, a neural tensor network for atomic relationship modeling, and a symbolic reasoning layer for rule-guided mineral intelligence. In addition, an explainable neuro-artificial intelligence technique incorporated to improve model interpretability and insight into predictions. The model is trained using the AdaBelief optimizer with quantile loss for ensure stable convergence and precise Mohs hardness prediction. The XDRL-MHP method validated utilizing the Comprehensive Database of Minerals, comprising 3,112 mineral instances with 140 mineralogical and physicochemical features. The simulation analysis of the XDRL-MHP model is performed using the Comprehensive Database of Minerals. Extensive comparative results show the effective performance of the XDRL-MHP model with an RMSE of 0.1140 over recent state-of-the-art models.**

***Keywords*—Mohs hardness prediction; mineral mining; adabelief optimizer; explainable artificial intelligence; physicochemical property**

*Corresponding author.

I. Introduction

Mineral identification is a key aspect of geological analysis. Traditional methods mainly rely on physical experiments or visual observation. Visual techniques, such as streak tests, powder color analysis, and HCl reactivity, depend on the skill of the evaluator and often require specialized instruments [1]. Both approaches are labor-intensive. Hardness is an important property of minerals, and Mohs hardness is one of the primary tests used for mineral identification. By using portable hardness picks, Mohs hardness can be measured efficiently and accurately. Different minerals can have significantly different Mohs hardness values [2]. For example, sphalerite and hematite have distinct hardness ranges but may appear similar in images. Therefore, hardness can serve as a key feature to differentiate them [3]. Hardness is related to the bond strength and composition of minerals. Light elements often form short and strong bonds, as do transition metals with higher valence bond density. Higher Mohs hardness is generally associated with stronger average bond interactions and higher bond density per unit volume [4]. Computational approaches combined with high-performance computing are used to understand deformation and compositional effects on hardness across different scales. Methods such as density functional theory, machine learning (ML), and molecular dynamics (MD) are commonly employed [5].

Several approaches were introduced, designed, and tested by numerous researchers to investigate Mohs hardness. Modeling methodologies reported in the literature are data-driven techniques (data compression, data prediction, and in-network processing). Statistical modeling and ML models are the most subjective algorithms in mineral prospectivity mapping [6]. These methods relied on the specialist's opinion or input data from the modeler to operate the weight computation of condition factors. These approaches are best for the unexplored landscapes categorized by certain known deposits [7]. But knowledge-based methodology is applied for any category of deposit utilizing fuzzy logic and the performance of the Dempster–Shafer evidence method. Data-driven algorithm offers an objective technique and highly depends on a connection between the predictors and the deposit types [8]. Hence, these

models are appropriate for moderate- to well-sampled regions characterized by known deposit forms. Deep learning (DL) classifiers are being broadly employed in a wide range of applications with diverse objectives in sections [9]. Some of the major limitations to be addressed are those that require higher computation complexity, as well as limited explicability and transparency, which mitigate confidence and decision verifiability made by a DL methodology. The lack of transparency and explicability in some regions is not unvaryingly an issue; later advanced techniques have a much higher precision [10]. Explaining Artificial Intelligence (XAI) is the field of research that aims to interpret, visualize, and explain the decisions taken by DL systems. Various researches have been conducted to understand how the approach makes its decisions; thus, in sensitive practical applications, the experts are optimistic in the method's predictions [11].

In spite of developments in mineral identification and hardness examination, standard experimental methodology remains time-consuming, labor-intensive, and rely heavily on professional interpretation. Recent ML and DL techniques for Mohs hardness prediction frequently need larger labeled datasets and exhibit limited generalization over different mineral classes. Existing methods often fail to learn complex mineral interactions and lack clear interpretability, which makes their predictions less reliable for geological use, so a more accurate and explainable model is needed for Mohs hardness prediction. To resolve these challenges, this manuscript presents an Explainable Deep Representation Learning Framework based on Mohs Hardness Prediction (XDRL-MHP). The following are major contributions of this research. A Key novelty for the proposed model is the construction of a physicochemical demonstration that explicitly integrates domain knowledge using atomic interactions, periodic dependencies, chemical affinities, and molecular relationships for mineral hardness prediction.

- Present a minimal redundancy maximal relevance (mRMR)-based feature selection (FS) strategy to identify the most informative mineralogical and physicochemical attributes for effective Mohs hardness prediction.
- Construct a comprehensive physicochemical representation module by integrating atomic interaction mapping, periodic table relationship encoding, chemical affinity representation, and molecular dependency to capture intrinsic mineral features.
- Design a neuro-symbolic hybrid architecture that combines a capsule network (CapsNet) module for hierarchical mineral pattern learning, a neural tensor network for atomic relationship modeling, and a symbolic reasoning layer for rule-guided mineral intelligence.
- Integrate an explainable neuro-artificial intelligence technique, including SHAP-based interpretation to quantify feature contributions and provide transparent, interpretable insights into model predictions.
- Employ the AdaBelief optimizer with quantile loss to ensure stable convergence and robust prediction performance.
- Perform the evaluation of the proposed XDRL-MHP model using the comprehensive database of Minerals and validate its predictive performance.

II. Existing Related Works on Mohs Hardness Prediction

The section briefly reviews the prior studies of Mohs hardness prediction along with existing research gaps. Ghadernejad and Esmaeili [12] designed predictive approaches for abrasivity and rock hardness according to hyperspectral imaging data, providing valuable data without interrupting the mining processes. Houshmand et al. [13] developed the outcome of an ML methodology for rock hardness prediction applying rock's geochemical and geophysical characteristics. Liu et al. [14] examined a ML system for predicting rock hardness employing morphological attributes. The results of this algorithm were used as the input for a meta-model, enduring linear fitting for predicting Mohs hardness, founding the Meta-RF and SVR model. In [15], the authors observed fractional chemical analysis following mechanical attrition, which shown distinctly various dimension-dependent distribution patterns including fluorite, REE, and barite minerals. Hadimani and Vanarotti [16] proposed an ML-based architecture to predict the Mohs hardness of minerals utilizing structural features and fundamental composition. Applying Scikit-learn, correlation analysis was conducted for identifying key predictors, and a Multi-Layer Perceptron Regressor (MLPRegressor) was implemented. Guo et al. [17] introduced a new multi-scale characterization technique. This methodology exclusively combines micro-zone X-ray diffraction analysis, nanoindentation technology, and ML strategies to technically examine micromechanical aspects of conglomerate instances from multiple areas. Cornu et al. [18] investigated the association among the mineralogical composition of the aggregates utilized in pavements and the long-term friction of the latter's surfaces. Sharifi Teshnizi et al. [19] discussed the drillability of granitic rocks by incorporating physical, petrographic, abrasivity, and mechanical parameters with ML and regression methodologies.

Although current research has enhanced rock and mineral hardness prediction through geochemical data, hyperspectral imaging, and machine learning, numerous difficulties still occur. Certain strategies rely on sensitive preprocessing stages or definite band-ratio attributes that may not completely extract compound physicochemical associations. Moreover, many techniques depend upon multi-sensor or instrument-heavy setups that minimize scalability in multiple mining situations, though image-based learning methodology frequently struggle with partial datasets and worse generalization across diverse mineral classes. Thus, recent models still struggle to effectually incorporate structural, compositional, and morphological data in a unified and consistent way for precise and interpretable Mohs hardness prediction.

III. Proposed Framework

The presented model introduces a robust framework for predicting Mohs hardness through mineralogical properties. The XDRL-MHP approach follows a systematic pipeline, integrating preprocessing, feature selection, feature representation, a neuro-symbolic hybrid model, explainable neuro-AI analytics, and model training. To prevent data leakage, the dataset was first split into training and testing sets. All normalization parameters and outlier processing criteria were resulting only from the training data. mRMR feature selection was also performed on the training set, and the selected features and pre-processing parameters were applied unchanged to the test set. The test set was kept hidden until the final validation. The structural overview of the proposed model is given in Fig. 1.

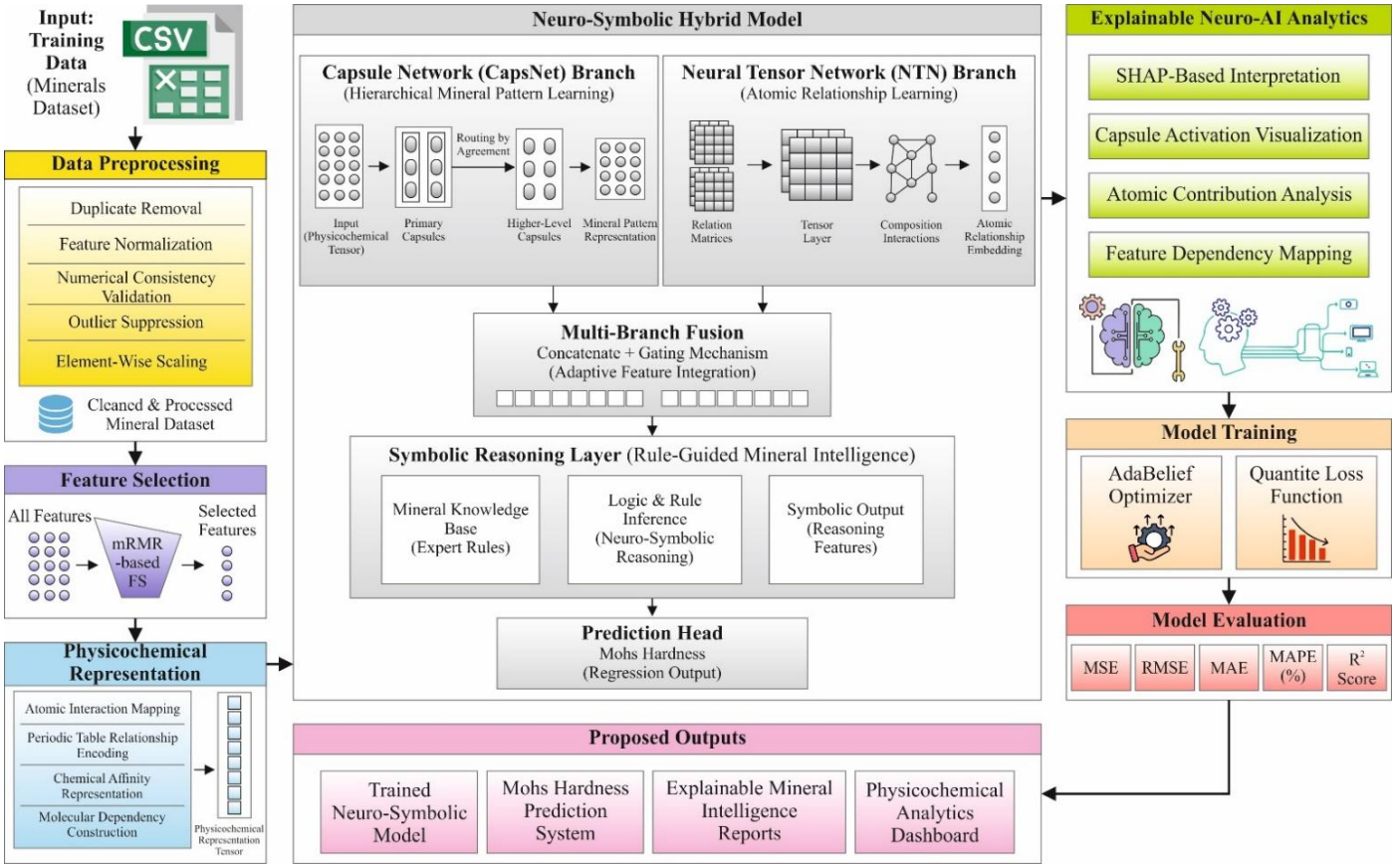

Fig. 1. Structural overview of the proposed model.

As depicted in Fig.1, the proposed model proceeds through a sequence of phases.

- Input data is pre-processed through duplicate removal, normalization using Z-score, consistency checking, outlier suppression, and element-wise scaling.
- An mRMR-based FS approach is employed to choose the most informative attributes while removing redundancy.
- Physicochemical representation utilizes an atomic interaction mapping, periodic table encoding, chemical affinity, and molecular dependency modeling.
- Neuro-symbolic hybrid model combines CapsNet for pattern learning, a neural tensor network for atomic relationships, and a symbolic reasoning layer for rule-guided intelligence.
- SHAP-based explainability is leveraged for quantifying feature contributions and improve model interpretability.
- AdaBelief optimizer with quantile loss was utilized for stable convergence and accurate prediction.

A. Data Preprocessing Pipeline

The data preprocessing stage ensures high-quality and consistent input for the model. It involves duplicate removal, consistency checking, outlier suppression, Z-score normalization, and element-wise scaling to enhance data reliability and model performance.

1) Duplicate removal: This process is an initial stage of preprocessing that focuses on eradicating duplicate reports from the data, which leads to improved reliability, and minimized redundancy formed by repeated entries or information gathered from various sources.

2) Z-score normalization: This normalization, also called standardization, converts data to have a mean of 0 and a unit variance of 1 [20]. It is extensively utilized for rescaling features so that they follow a standard normal function. This

model minimizes the effect of varying feature scales and enhances numerical stability in learning models.

$$x_{norm} = \frac{X - \mu}{\sigma} \quad (1)$$

In this Eq. (1), X implies the real feature data, μ implies the mean of the attribute, σ implies the SD of the attribute, and X_{norm} indicates the scaling data.

3) Numerical consistency validation: This is another pre-processing stage that assures each numerical value in the data is within valid ranges, domain-specific rules, and suitable data types. For example, it verifies that no negative ore grades and valid coordinate ranges.

$$x \in [x_{\min}, x_{\max}] \quad (2)$$

If violated, data are corrected, removed, or imputed.

4) Outlier suppression: It minimizes the effect of extreme values that deviate considerably from the complete data distribution, enhancing model stability. Depend on the IQR-based rule:

$$IQR = Q3 - Q1 \quad (3)$$

$$x < Q1 - 1.5 \cdot IQR \text{or} x > Q3 + 1.5 \cdot IQR \quad (4)$$

Certain values are clipped or eliminated (winsorized).

5) Element-wise scaling: Element-wise scaling is a preprocessing method where every feature is independently converted to a common scale to ensure equal contribution in model training.

$$x' = f(x) \quad (5)$$

Here, $f(\cdot)$ denotes a scalar operation used distinctly for all features.

B. mRMR-Driven Feature Selection Strategy

The mRMR-based FS technique was employed to recognize the most significant mineralogical attributes for Mohs hardness prediction. It improves prediction performance by maximizing feature relevance while minimizing redundancy among selected features [21].

1) Maximal relevance: Based on mRMR, the highest relevance is reached by obtaining a feature subset that fulfills Eq. (6), increasing the average of the mutual information (MI) among the attributes in the feature subset and the target variable.

$$\max D = \frac{1}{|K|} \sum_{x_i \in K} I\,(xi; y) \quad (6)$$

here χ_i denotes the feature, y indicates the target variable, and K refers to the subset of features. D implies the average of the MI between the aspects and the target variable, and I points out the MI between the feature x_i and the target variable y.

$$I(x,y) = \iint \mathrm{p}\,(x,y) log \frac{p(x,y)}{p(x)p(y)} dxdy \quad (7)$$

here $p(y)$ implies the marginal probability distribution of χ and y; $p(x,y)$ indicates the joint probability distribution of χ and y and $p(x)$.

2) Minimal redundancy: During feature subset selection based solely on the maximum relevance criterion, a substantial amount of redundant information is retained among the selected attributes. This redundancy could impact the computational effort needed by the method and potentially reduce the prediction accuracy.

$$\min R = \frac{1}{|K|^2} \sum_{x_j x_i \in K} I\left(x_{i;} \cdot x_j\right) \quad (8)$$

Here, x_i and χ_j point out the features, I implies the MI among the features, and K indicates the subset of features.

$$\max \Phi = D - R \quad (9)$$

Φ implies the variance between redundancy and relevance. By increasing the variance between redundancy and relevance, the mRMR could minimize redundancy in the subset of features, while preserving higher relevance. Consider that the $n-1$ selects from the actual feature set X, constitute the subset K_{n-1}, then the selection of the n_{th} feature x_n.

$$x_n \in XK_{n-1} \max \left\{ I\left(x_{n;} \cdot y\right) - \frac{1}{n-1} \sum_{x_j \in K_{n-1}} I\left(x_{n;} \cdot x_j\right) \right\} \quad (10)$$

The mRMR sequentially chooses attributes from the remaining set of features $X - K$ and adds them to the subset K.

C. Physicochemical Representation

It is a feature engineering method that encodes chemical and mineralogical data into structured interpretations for enhanced learning.

1) Atomic interaction mapping: It extracts the interaction patterns among atoms that depend on their bonding behavior and spatial correlations in mineral structures. This helps to understand how many components impact one another in a compound.

2) Periodic table relationship encoding: It encodes elemental features by applying periodic table properties, including group, period, and atomic number.

3) Chemical affinity representation: It represents the tendency of components to interact based on their chemical reactivity and compatibility. It facilitates identifying stronger and weaker elemental connections among minerals.

4) Molecular dependency construction: It incorporates chemical affinities and atomic interactions to create a structured molecular association graph. To enhance mineral representation learning, extract the overall dependency between atoms.

For reproducibility, the physicochemical representation is formally defined as $R = [A; P; C: M]$, where A, P, C, and M represent the atomic interaction, periodic table, chemical affinity, and molecular-dependency depiction, respectively. For a mineral including n constituent element, the stomic interaction matrix is defined as $A_{ij} = f\left(a_i, a_j\right)$, whereas the periodic

illustration is encoded as $P_i = [Z_i, G_i, T_i]$, where Z_i, G_i and T_i represent atomic number, group, and period. The chemical-affinity representation is attainare as $C_{ij} = g(a_i, a_j)$ and molecular relationships is built as $M_{ij} = h(A_{ij}, C_{ij})$. These representations are concatenated to form the final feature vector utilized by the neuro-symbolic method.

D. Neuro-Symbolic Hybrid Model

The neuro-symbolic hybrid model is designed to effectively capture both data-driven patterns and rule-based reasoning in mineralogical analysis. It integrates CapsNet for hierarchical pattern learning, a neural tensor network for atomic relationship modeling, and a symbolic reasoning layer for rule-guided intelligence.

1) Capsule network: The CapsNet is a neural network (NN) framework that denotes features as vectors in capsules that capture the presence and spatial correlation [22]. Unlike image-based applications, the capsules in the proposed model do not signify physical spatial locations. Instead, they group associated mineralogical and physicochemical features into large-scale feature representations. The routing mechanism supports the method in preserving and integrating these feature dependencies, which is useful for modeling interactions between elemental, periodic, and chemical properties.

It employs dynamic routing and hierarchical feature dependencies for increasing the representation learning. The adaptable spatial capsule unit has been utilized to acquire higher-level feature representations by obtaining the hierarchical correlation from the mineralogical information. The feature set is systematized as numerous capsules, in which each capsule encodes a different spatial–semantic pattern of the input. The transformation from low-level to high-level capsules can be executed by employing the shared weight matrix:

$$u_{j|i}^{(a+x)(b+y)} = W_{ij}^{xy} u_i^{(a+x)(b+y)} \tag{11}$$

Here, the term $u_{j|i}^{(\mathrm{a+x})(\mathrm{b+y})}$ signifies the j^{ih} features predicted in the layer. The weighted summation of all $(a + x, b + y)$ capsules is derived from $u_{j|i}$, thereby representing that the vectorized prediction must be calculated as the capsule's input, as given below:

$$I_j^{ab} = \sum_i \sum_x \sum_y Q_{ij}^{xy} \, u_{j|i}^{(a+x)(b+y)} \tag{12}$$

Here, the parameter I_j^{ab} signifies the capsule j input vector, and the term Q_{ij}^{xy} denotes the coupling coefficient. The interpretations are accomplished by the softmax function and dynamic routing method:

$$Q_{ij}^{xy} = \frac{\exp\left(R_{ij}^{xy}\right)}{\Sigma_{j=1}^{P} R_{ij}^{xy}} \tag{13}$$

From this mathematical term P signifies the overall counts of posterior layer capsules v. At the beginning of the training process, the term R_{ij}^{xy} is set to 0, the parameter R_{ij}^{xy} can be iteratively advanced by parameters for agreement with prediction vectors $u_{j|i}^{(a+x)(b+y)}$ and v_j^a. Accordingly, the capsule $u_{j|i}^{(a+x)(b+y)}$ gives improved capsule prediction v_j^{ab} and the major rise is achieved to R_{ij}^{xy} as given below:

$$R_{ij}^{xy} \leftarrow R_{ij}^{xy} + u_{j|i}^{(a+x)(b+y)} v_j^{ab} \tag{14}$$

For the reduction of the capsule output, the non-linear function can be utilized to compress the input vector, and its mathematical form is given by:

$$v_j^{ab} = Squash(I_j^{ab}) \tag{15}$$

The output capsule vector $v_j^{ab}$is encoded as the final hierarchical mineral representation and was employed for Mohs Hardness classification.

2) Neural tensor network: The neural tensor network is an NN developed to model intricate relationships among two input feature vectors by applying the tensor-based bilinear transformation. This can be broadly employed to obtain important relative dependencies during the representation learning process. The relationship between 2 feature vectors x and y can be measured by,

$$h = \tanh\left(x^T W^{[1:K]} y + V[x; y] + b\right) \tag{16}$$

In this mathematical form, the term $W^{[1:K]}$ refers to the 3rd-order tensor that gains multiplicative correlation, the term V represents the weight matrix for linear transformation, the factor b indicates the bias vector, and the term $[x; y]$ signifies concatenation. The non-linear activation function allows the model to obtain higher-order feature interactions. The tensor factor permits pairwise feature relationships as clearly designed over numerous latent dimensions. It generates the NTN, which is especially efficient for obtaining intricate dependencies in organized information. The final output score for prediction can be measured by:

$$s = u^T h \tag{17}$$

Now, the parameter u refers to the learnable parameter, the term h indicates the hidden representation for the final prediction score.

3) Symbolic reasoning layer: The Symbolic Reasoning Layer incorporates rule-based symbolic AI with DL to allow structural and interpretable mineral information. This can be encoded in the geological details in a clear, logical set of rules, thereby permitting domain-driven reasoning across the mineral features when adding data-driven feature learning. This integration increases the interpretability and predictive consistency in mineral evaluation processes. The symbolic rule aggregation method can be measured by:

$$R(x) = \sum_{i=1}^{n} \omega_i \, r_i(x) \tag{18}$$

From this mathematical form, the factor ω_i signifies their resultant importance weights or confidence, and the term $r_i(x)$ signifies individual geological or symbolic rules utilized for the

input x. The final prediction, has combined the symbolic reasoning and DL outputs, can be represented by:

$$y = \sigma\big(f_\theta(x) + \lambda R(x)\big) \quad (19)$$

Here, the term $R(x)$ points to the outcome of the symbolic reasoning, term $f_\theta(x)$ refers to the output NN, and the mathematical notations λ and σ indicate the symbolic layer and activation function that generate the final mineral prediction. Fig. 2 signifies the design of the neuro-symbolic hybrid model.

The symbolic reasoning layer combines domain-informed rules depending on the relationships between elemental composition, atomic interaction, periodic properties, and chemical affinity. These rules are incorporated with the neural network output using weighted rule aggregation to give interpretable mineralogical reasoning. The contribution of the symbolic reasoning module is validated through the ablation study by comparing the complete XDRL-MHP technique with a variant without symbolic reasoning under the same experimental environments.

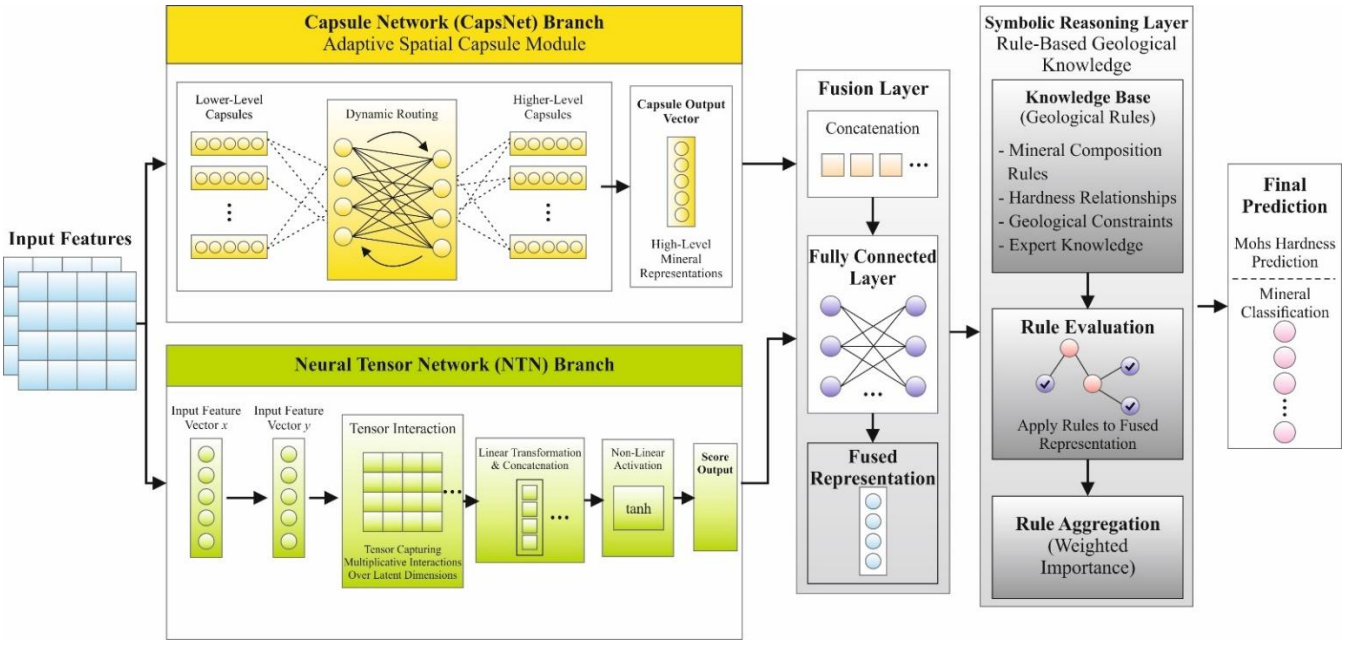

Fig. 2. Design of neuro-symbolic hybrid model.

E. Explainable Neuro-AI Analytics

SHAP is an explainable AI technique used to interpret model predictions by quantifying the contribution of each feature to the final output. It is an integrated explainability architecture proposed by Lee and Lundberg that interprets the prediction of any ML strategy by allocating every attribute a significance value for a certain record [23]. It depends on the model of Shapley values from cooperative game theory, here, all attributes are addressed as "players" contributing to the last prediction. It associates local explanation algorithms like LIME with the theoretical basis of Shapley values, delivering a reliable and explainable decomposition of method outcomes. The SHAP explanation system illustrates the prediction as an additive composition of feature contributions, represented as:

$$g(z') = \phi_0 + \sum_{j=1}^{M} \phi_j z'_j \quad (20)$$

Here ϕ_0 indicates the base value, $g(z')$denotes the explanation model, $z'_j \in \{0,1\}$represents a simplified binary representation indicating whether feature j is present in the coalition or not, and $\phi_j$points out the SHAP value representing the contribution of feature j. Mimplies the total count of attributes. Based on the Shapley value formulation, the SHAP value $\phi_j$is calculated:

$$\phi_j = \sum_{S \subseteq F \setminus \{j\}} \frac{|S|!(M - |S| - 1)!}{M!} [f(S \cup \{j\}) - f(S)] \quad (21)$$

Here, S denotes all possible feature subsets not containing feature j, and F refers to the full feature set. This formulation determines the average marginal significance of attributes j over each possible coalition.

F. Model Training

AdaBelief is an adaptive optimizer approach that updates method parameters by integrating a momentum-driven gradient estimator with a difference evaluation based on gradient deviation [24]. The optimization starts with the calculation of the gradient $g_t = \nabla f(\theta_t)$ that signifies the direction of steepest descent of the loss function. The 1st-order momentum is then upgraded as

$$m_t = \beta_1 m_{t-1} + (1 - \beta_1) g_t \quad (22)$$

The 1st-order momentum takes the exponential average direction of previous gradients. At the same time, AdaBelief proposes an improved 2nd-order momentum that evaluates the belief within the gradient for tracking the deviation from the 1st moment, expressed as follows:

$$s_t = \beta_2 s_{t-1} + (1 - \beta_2)(g_t - m_t)^2 \quad (23)$$

To eliminate initialization bias, two moments are modified as

$$\widehat{m}_t = \frac{m_t}{1-\beta_1^t}, \hat{s}_t = \frac{s_t}{1-\beta_2^t} \quad (24)$$

At last, the parameters are updated employing an adaptive learning rate rule computed by:

$$\theta_{t+1} = \theta_t - \eta \cdot \frac{\widehat{m}_t}{\sqrt{\hat{s}_t} + \epsilon} \quad (25)$$

In this Eq. (25), η denotes the learning rate and ϵ implies a smaller constant for numerical stability. The pseudocode of the AdaBelief optimizer is represented in Algorithm 1.

Algorithm 1: Pseudocode of AdaBelief Optimizer

Input: Learning rate α, decay rates β_1, β_2, stability constant ϵ
Output: Upgraded parameters x_{t+1}
Set: x_0, $m_0 = 0$, $s_0 = 0$
For $t = 1$to Tdo:
The gradient has been calculated as
$g_t = \nabla f_t(x_t)$The 1st moment is updated as

$m_t = \beta_1 m_{t-1} + (1-\beta_1) g_t$The 2nd moment is updated as

$s_t = \beta_2 s_{t-1} + (1-\beta_2)(g_t - m_t)^2$Bias-corrected estimation was calculated as

$$\widehat{m}_t = \frac{m_t}{1-\beta_1^t}, \hat{s}_t = \frac{s_t}{1-\beta_2^t}$$

The parameters are updated employing an adaptive scaler as
$x_{t+1} = x_t - \frac{\alpha\, \widehat{m}_t}{\sqrt{\hat{s}_t}+\epsilon}$Return x_{t+1}

The model utilizes Quantile Loss to enhance robustness and attain precise Mohs hardness prediction by lessening asymmetric prediction errors.

$$L_q(y, \hat{y}) = \max\big(q(y-\hat{y}), (q-1)(y-\hat{y})\big) \quad (26)$$

where, y denotes the actual hardness value, $\hat{y}$ implies the predicted hardness value, and q signifies the quantile parameter controlling error weighting.

Quantile Loss to enhance the robustness of Mohs hardness prediction, quantile loss was used as the regression objective with $\tau = 0.5$. The quantile loss is defined as:

$$L_\tau(y, \hat{y}) = \begin{cases} \tau(y, \hat{y}) & y \geq \hat{y} \\ (1-\tau)(\hat{y} - y) & y < \hat{y} \end{cases}$$

The value of $\tau = 0.5$ was selected depending on validation performance. Its efficiency was compared with MSE and MAE under identical training and evaluation conditions.

Table I illustrates the data standardized using Z-score normalization and IQR-based outlier suppression. mRMR was used to select relevant features, denoted by four chemical dependencies. The method integrates CapsNet with dynamic routing and NTN, followed by multi-branch fusion and rule-guided reasoning. Training utilized AdaBelief, quantile loss, batch size 32, and epochs 25, learning rate 0.001with early stopping.

TABLE I. PARAMETER CONFIGURATION OF XDRL-MHP METHOD WITH TRAIN -TEST SET

Category	Parameter	Setting
Preprocessing	Normalization	Z-score
	Outlier handling	IQR-based suppression
Feature Selection	Method	mRMR
Feature Representation	Representation methods	Atomic interaction, periodic relationship, chemical affinity, molecular dependency
Model	Capsule branch	CapsNet with dynamic routing
	Relationship branch	Neural Tensor Network (NTN)
	Fusion	Multi-branch fusion
	Reasoning	Rule-guided symbolic reasoning
Training	Optimizer	AdaBelief
	Loss function	Quantile Loss
	Quantile Value	0.5
	Learning Rate	0.001
	Batch size	32
	Epochs	25

IV. EXPERIMENTAL ANALYSIS AND DISCUSSION

The empirical evaluation of the XDRL-MHP method was conducted using the Comprehensive Database of Minerals [25]. This dataset contains 3112 minerals along with their chemical compositions, crystal structures, and physical and optical characteristics. The dataset also includes several properties such as crystal structures, Mohs Hardness, Specific Gravity, Molar Volume, Optical axes, Optical dispersion, and Calculated Density. A total of 140 features, 88 features were selected for training. The experiments were conducted utilizing a 70:30 training–testing split. The method was executed through Python 3.11 and trained on a system equipped with an NVIDIA RTX 4090 GPU (24 GB VRAM), Intel Core GPU (24 GB VRAM), Intel Core i9 processor, and 32 GB RAM. The training configuration and hardware settings were kept consistent for all experiments to ensure a fair comparison.

Fig. 3 presents the correlation heatmaps analysis of the selected 88 mineral properties, which were effectively structured into six groups, enabling a clear understanding of the correlation pattern. In particular, chemically related elements and rare earth elements exhibit a well-defined correlation pattern. The result indicates a strong and positive correlation; the analysis reveals a well-structured relationship among several feature groups, making it suitable for advanced statistical evaluation.

Fig. 4 shows the statistical distribution of Mineralogical and Physicochemical properties used for Mohs Hardness Prediction. The result shows that the categorical variables, such as crystal structure and diaphaneity, show discrete patterns. Elemental variables such as hydrogen and helium show a highly imbalanced distribution with limited variation. In particular, the variation in physical and optical characteristics delivers essential information for accurate Mohs hardness prediction in the mineral dataset.

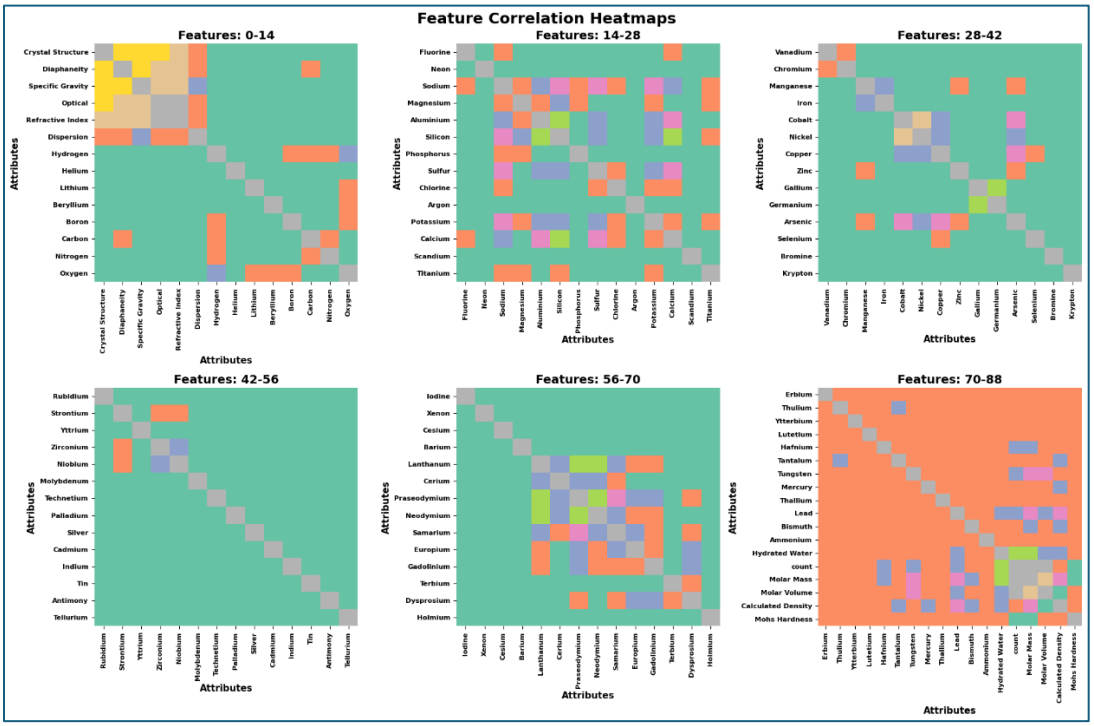

Fig. 3. Feature correlation heatmaps analysis.

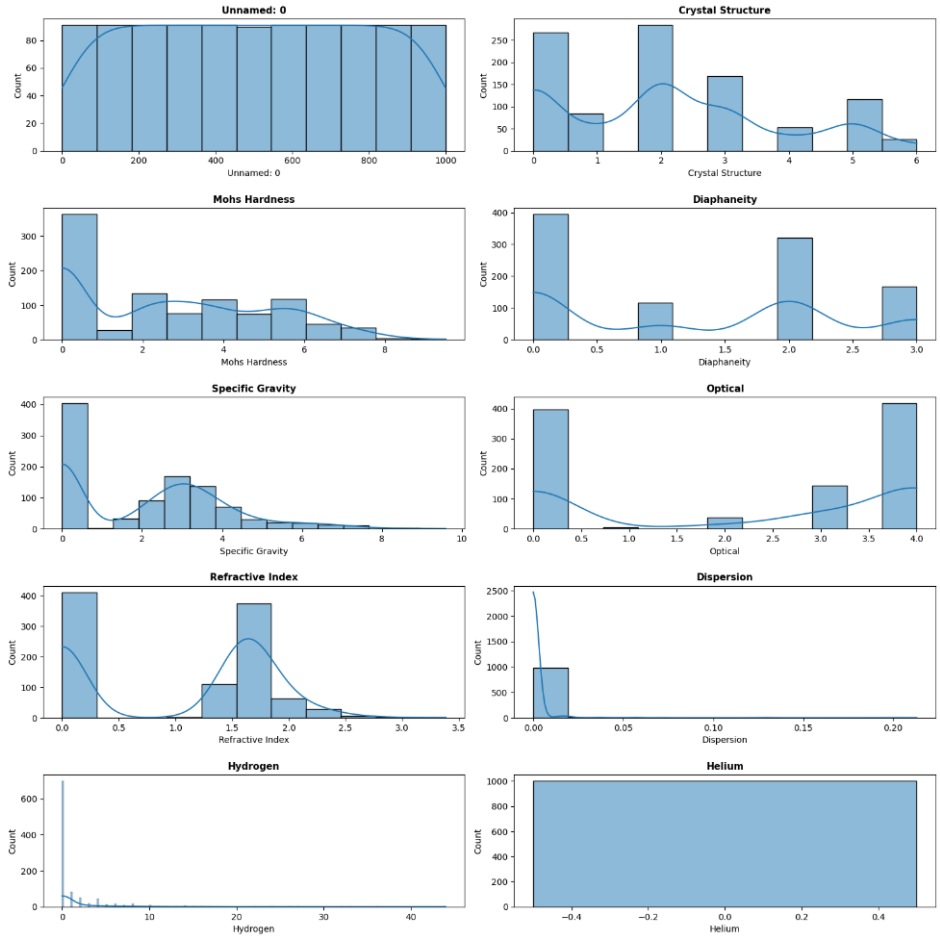

Fig. 4. Statistical distribution of mineralogical and physicochemical properties.

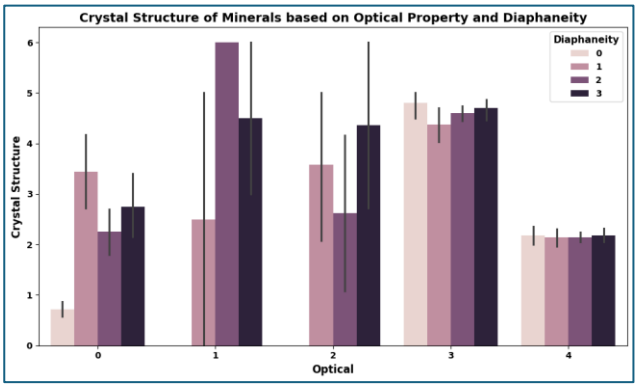

Fig. 5. Analysis of the crystal structure of various minerals based on optical properties and diaphaneity.

Fig. 5 displays the analysis of the crystal structure of various minerals based on optical properties and diaphaneity. Higher optical and diaphaneity values indicate a more stable and complex crystal structure, while low values exhibit high variation in structural pattern. Therefore, the result highlights the strong interrelationships among these attributes, which makes them suitable for mineralogical analysis and accurate Mohs hardness prediction.

Fig. 6 illustrates the Mohs hardness prediction of minerals using training and testing splits. The graph shows prediction behavior at different epochs (10, 15, 20, and 25), and the predictions are compared with actual hardness values for both training and testing datasets.

Next, Fig. 7 presents the loss curve analysis of the XDRL-MHP model with diverse evaluation metrics across the train-test split. The MSE, RMSE, and MAE gradually decrease with more epochs, displaying better learning and minimized errors, while R^2 increases and MAPE stabilizes after early fluctuations, which indicates steady convergence and better overall performance.

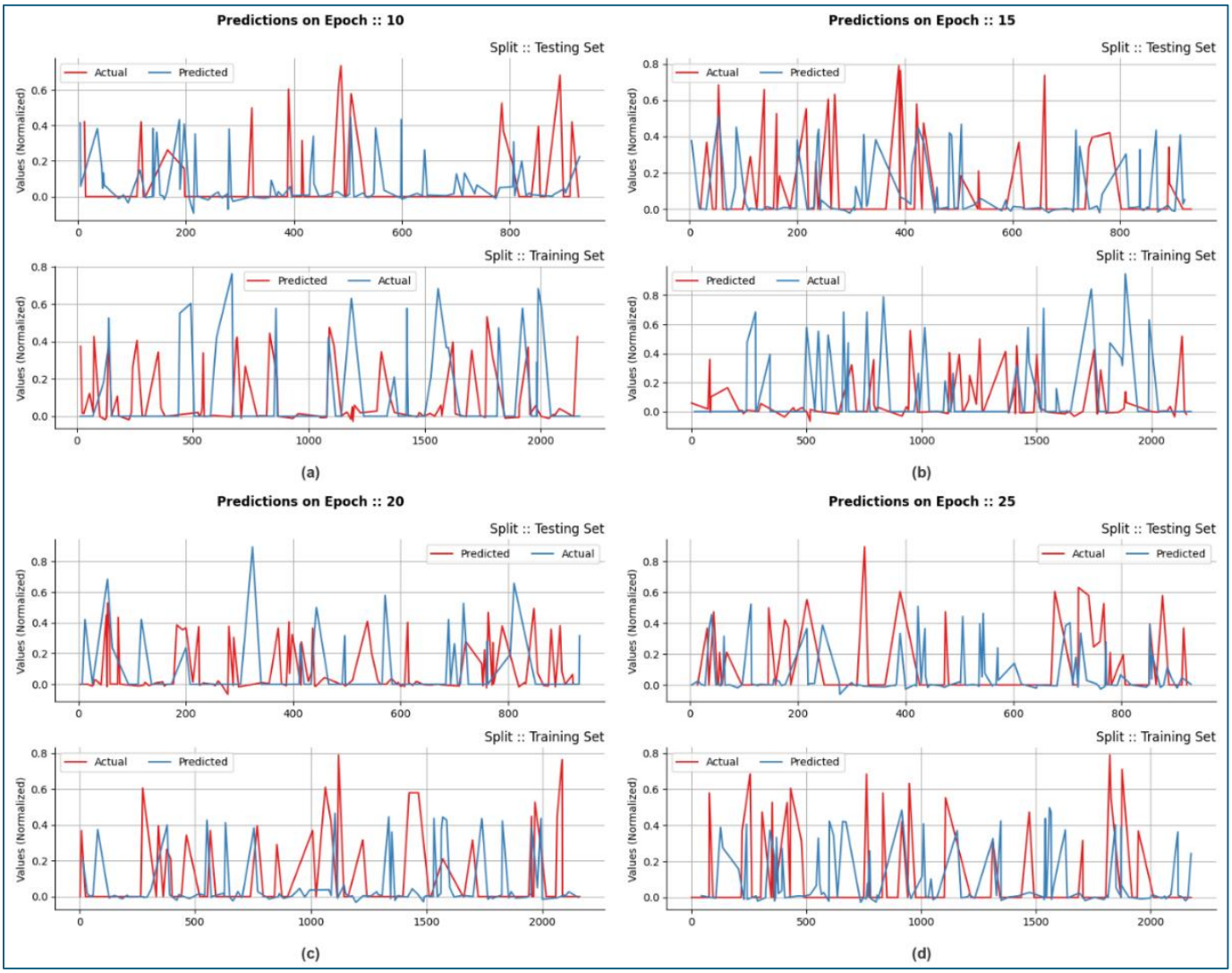

Fig. 6. Mohs hardness prediction of minerals using train- test splits.

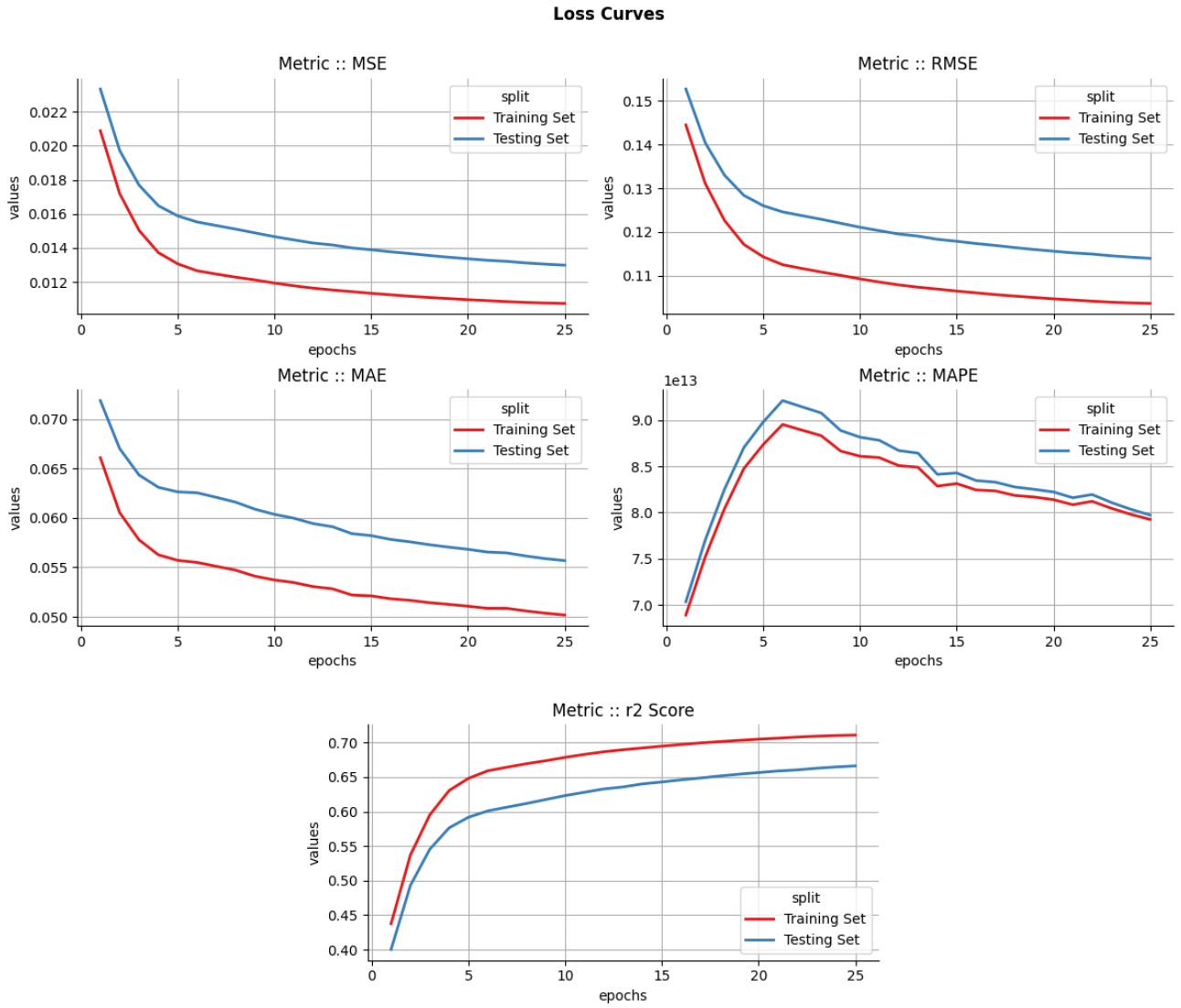

Fig. 7. Loss curve of the XDRL-MHP method with metrics.

TABLE II. MOHS HARDNESS PREDICTION ANALYSIS OF XDRL-MHP METHOD WITH TRAIN -TEST SET

Metrics	Training Set	Testing Set
MSE	0.0107	0.0130
RMSE	0.1036	0.1140
MAE	0.0502	0.0557
MAPE	7.9261	7.9736
r2 Score	0.7109	0.6662

Table II and Fig. 8 exhibit the Loss curve and performance metric analysis of the XDRL-MHP model for both the training and testing sets over 25 epochs. The gradual decrease in error values shows that the model achieves improved learning efficiency and low prediction loss. Simultaneously, the continuous increase in R^2 score value indicates stable learning behaviour and improved model accuracy, which shows strong predictive capability for Mohs hardness estimation.

Fig. 8. Mohs hardness prediction analysis of XDRL-MHP approach with training and testing set.

TABLE III. COMPARATIVE ANALYSIS OF THE XDRL-MHP SYSTEM WITH EXISTING METHODS

Models	RMSE	MAE	MAPE	r2 Score
kNN	2.3195	1.8600	12.9300	0.5770
AdaBoost	2.4413	1.9600	24.7800	0.5534
GradientBoost	1.4663	1.1650	27.7500	0.5499
MLP	2.0905	1.4860	15.1700	0.6112
ANN-TLBO	0.6782	0.2210	21.6300	0.5209
Transformer	1.9647	2.3300	13.7100	0.5280
ConvLSTM	2.0075	0.9230	8.5500	0.6334
VGG16	2.1354	1.6200	15.5700	0.6163
XDRL-MHP	0.1140	0.0557	7.9736	0.6662

Table III and Fig 9 present the comparative performance analysis of the proposed XDRL-MHP model with various metrics [26, 27]. Traditional models such as KNN and AdaBoost show higher RMSE and MAE values, which indicates lower prediction accuracy. Models such as MLP, Transformer, ConvLSTM, and VGG16 exhibit better learning capabilities compared to traditional methods, but show lower performance than the proposed model. The proposed XDRL-MHP outperforms all existing approaches by achieving RMSE (0.1140), MAE (0.0557), MAPE (7.9736), and R2 score (0.6662). The result highlights that the model achieves the most reliable and accurate Mohs hardness prediction.

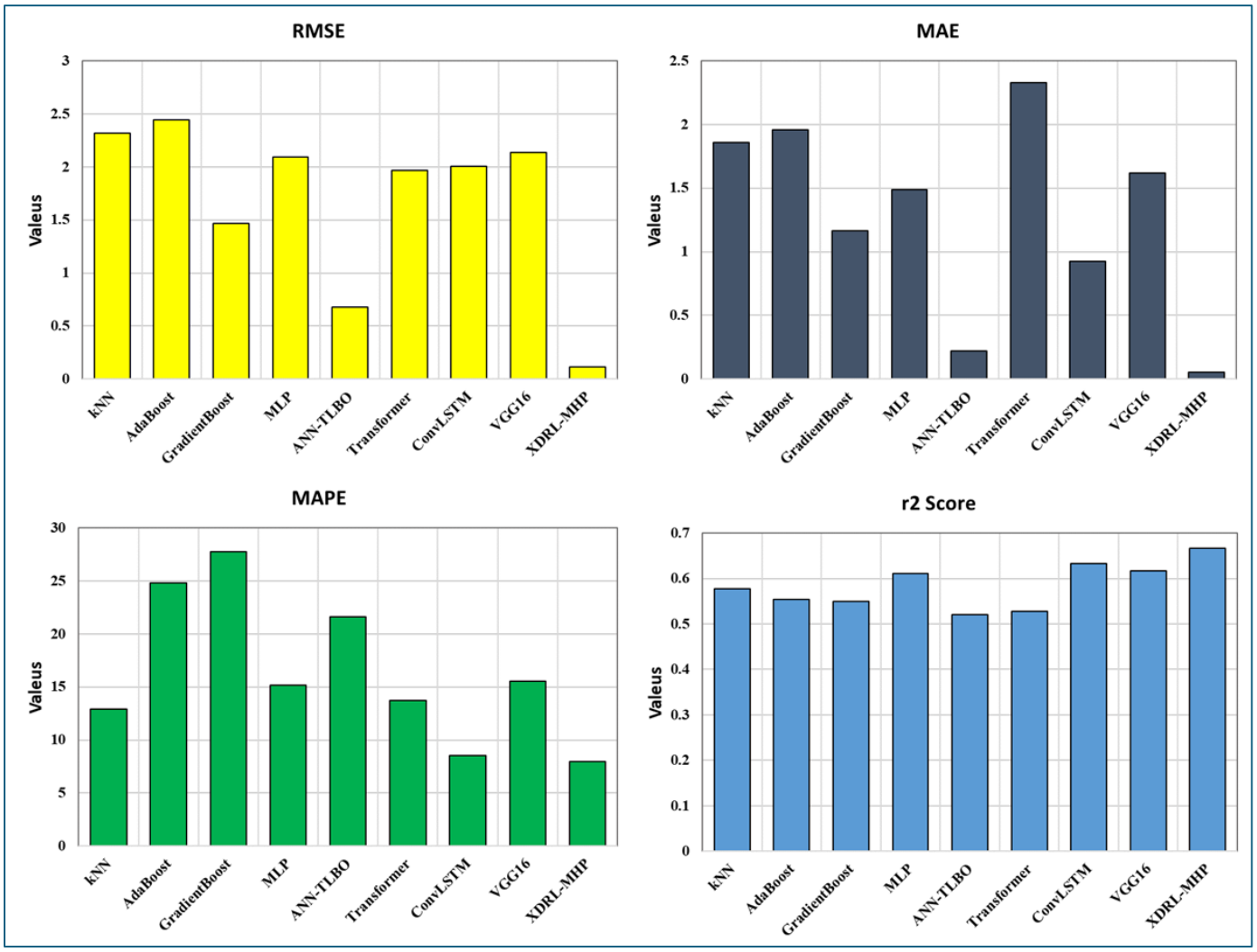

Fig. 9. Comparative results of the XDRL-MHP method with metrics.

An ablation study assesses how different parts of a method influence its performance by testing the classification with specific models removed or altered. This precedure provides which modules are significant and which have less impact. By comparing results, investigators gain insight into the model's behavior. These results enable better design and optimization. Table IV demonstrates the ablation study of the XDRL-MHP technique. The results show that Baseline, mRMR (Minimum Redundancy Maximum Relevance), mRMR + Physicochemical Representation (PR), mRMR + PR + MLP + Neural Tensor Network (NTN), mRMR + PR + Residual Network + Neural Tensor Network (NTN), and mRMR + PR + Capsule Network + Neural Tensor Network (NTN) models have attained higher performance under different metrics. In the meantime, the XDRL-MHP (Explainable Deep Representation Learning Framework for Mohs Hardness Prediction) method has got less performance, with RMSE of 0.114, MAE of 0.0557, MAPE of 7.9736, and R^2 score of 0.6662.

TABLE IV. ABLATION STUDY ANALYSIS OF THE XDRL-MHP METHOD

Configuration	RMSE	MAE	MAPE	R^2 Score
Baseline	0.1867	0.1094	14.8265	0.4728
mRMR(Minimum Redundancy Maximum Relevance)	0.1624	0.0915	12.8462	0.5517
mRMR + Physicochemical Representation (PR)	0.1458	0.0796	10.9473	0.5984
mRMR + PR + MLP + Neural Tensor Network (NTN)	0.1336	0.0724	9.9148	0.6271
mRMR + PR + Residual Network + Neural Tensor Network (NTN)	0.1271	0.0671	9.2846	0.6438
mRMR + PR + Capsule Network + Neural Tensor Network (NTN)	0.1237	0.0648	8.9135	0.6519
XDRL-MHP (Explainable Deep Representation Learning Framework for Mohs Hardness Prediction)	0.114	0.0557	7.9736	0.6662

TABLE V. COMPUTATIONAL EFFICIENCY OF THE XDRL-MHP MODEL

Model	Parameters(M)	GFLOPs	Inference Time (ms)
MLP	0.42	0.18	2.84
ANN-TLBO	0.58	0.27	3.21
Transformer	2.84	1.46	6.73
ConvLSTM	3.72	2.18	8.41
VGG16	14.72	15.50	12.48
XDRL-MHP	**0.31**	**0.14**	**2.17**

Table V depicts the computational efficiency of the XDRL-MHP method compared with other algorithms. Based on inference time, the XDRL-MHP model gives minimum value of 2.17ms, Flops of 0.14G and parameters of 0.31M whereas the MLP, ANN-TLBO, Transformer, ConvLSTM, and VGG16 techniques gain better time of 58.60ms, 0.42ms, 0.58ms, 2.84ms, 3.72ms, and 14.72ms, correspondingly.

Table VI illustrates that the proposed method was validated utilizing 10-fold cross-validation to evaluate its reliability and stability. The proposed model obtained a mean RMSE of 0.1135, MAE of 0.055, and MAPE of 7.816%, demonstrating comparatively low prediction error. The mean R^2 score was 0.6613, representing better predictive performance.

The low standard deviations (STD), particularly ±0.0029 for RMSE and ±0.0092 for R^2, specify continuous performance across all folds.

Fig. 10 illustrates the SHAP-Based analysis for explainable Mohs Hardness Prediction using global feature importance and local explanation summary. Among all parameters, the refractive index, optical properties, and specific gravity are the most influential parameters that contribute to prediction accuracy. The local explanation further improves model transparency and support to understand the feature-level behavior. Features with positive SHAP values support higher predictions, while negative values decrease the prediction output. This SHAP analysis enhances model transparency and strengthens reliable model decision-making.

TABLE VI. CROSS-VALIDATION ANALYSIS OF THE XDRL-MHP METHOD

Fold	RMSE	MAE	MAPE (%)	R^2 Score
Fold 1	0.109	0.0521	7.421	0.648
Fold 2	0.112	0.0543	7.683	0.657
Fold 3	0.115	0.0558	7.912	0.664
Fold 4	0.111	0.0539	7.584	0.653
Fold 5	0.117	0.0571	8.146	0.672
Fold 6	0.113	0.0548	7.756	0.661
Fold 7	0.116	0.0564	8.031	0.668
Fold 8	0.118	0.0575	8.214	0.676
Fold 9	0.110	0.0529	7.513	0.651
Fold 10	0.114	0.0551	7.902	0.663
Mean	**0.1135**	**0.055**	**7.816**	**0.6613**
STD (±)	**0.0029**	**0.0015**	**0.269**	**0.0092**

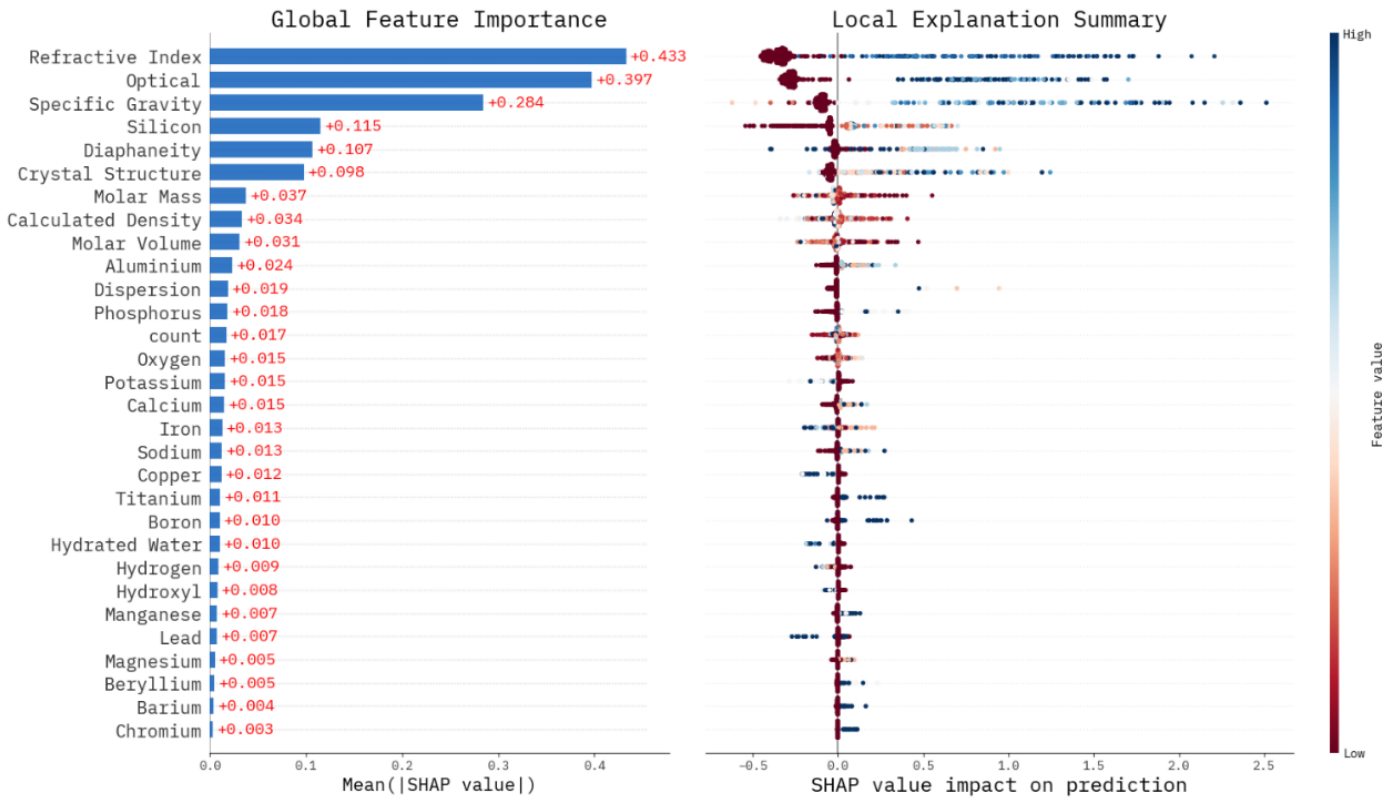

Fig. 10. SHAP-based analysis for explainable Mohs Hardness Prediction.

The experimental outcome shows that the proposed XDRL-MHP architecture effectively forecasts Mohs hardness utilizing mineralogical and physicochemical properties. The incorporation of mRMR-based feature extraction and physicochemical selection learning enhances the extraction of discriminative mineral attributes. Furthermore, the neuro-symbolic hybrid framework improves the ability to extract composite atomic interactions and structural dependencies, causing enhanced prediction stability and accuracy. The integration of explainable neuro-AI further delivers the best transparency and interpretability in the prediction method.

V. Conclusion and Future Work

This study has presented an XDRL-MHP approach for predicting Mohs hardness using mineralogical properties by modeling mineral composition and structural characteristics. The proposed model utilizes mRMR for FS to recognize the most informative physicochemical attributes. A physicochemical representation is constructed utilizing atomic interaction mapping, periodic table relationship encoding, chemical affinity representation, and molecular dependency construction for capturing intricate mineral relationships. Subsequently, a neuro-symbolic hybrid framework is designed, and an explainable neuro-AI model is integrated to enhance model interpretability and insight into predictions. The model is trained utilizing the AdaBelief optimizer with quantile loss to ensure stable convergence and precise Mohs hardness prediction. The experimental analysis of the XDRL-MHP model is performed using the Comprehensive Database of Minerals. Extensive comparative results show the effective performance of the XDRL-MHP model with an RMSE of 0.1140 over existing approaches. Even though the proposed method displays stronger prediction outcomes, it is restricted by reliance on a particular mineralogical database that might impact generalization. It also lacks multi-modal data incorporation and sophisticated graph- or transformer-driven learning for a deeper atomic relationship model. In future studies, the structure could be improved using larger and more diverse datasets to improve the performance of the method. Furthermore, integrating advanced DL and XAI approaches could further improve prediction accuracy and interpretability.

Data Availability Statement

The data that support the findings of this study are openly available in the Kaggle repository at https://www.kaggle.com/datasets/vinven7/comprehensive-database-of-minerals/data [25].

Acknowledgment

The authors extend their appreciation to Northern Border University, Saudi Arabia, for supporting this work through project number (NBU-CRP-2026-540). The authors are thankful to the Deanship of Graduate Studies and Scientific Research at the University of Bisha for supporting this work through the Fast-Track Research Support Program.

References

[1] Çoban, E. And Saplıoğlu, K., 2025. Predicting Water Hardness Through Data-Driven Intelligence: A Comparative Machine Learning Approach. Konya Journal of Engineering Sciences, 13(4), pp.1094-1106.

[2] Ghadernejad, S., Esmaeili, K. and Consens, M.P., 2025. Sensor-Based Rock Hardness Characterization in a Gold Mine Using Hyperspectral

Imaging and Portable X-Ray Fluorescence Technologies. Remote Sensing, 17(12), p.2062.

[3] Chowdhury, M., Shrima, S.R. and Islam, M.S., 2025. Comparative analysis of deep learning architectures for multi-class mineral classification: a study using EfficientNet and ResNet models. Earth Science Informatics, 18(3), p.485.

[4] Liu, H., Zhao, Z., Ma, Q., Du, J. and Liu, X., 2025. Cross-scale correlation analysis of water-induced deterioration on soft rock in coal mine underground reservoir engineering based on deep learning algorithm. International Journal of Coal Science & Technology, 12(1), p.48.

[5] Han, L., Shi, X., Ni, H., Jiang, S., Che, M. and Qu, F., 2025. Fracture toughness evaluation of shale based on machine learning and micromechanical approach. Engineering Fracture Mechanics, 323, p.111194.

[6] Gupta, R. and Bhui, U.K., 2026. Predicting complex mineralogy in oil and gas drilling: a support vector machine learning model using integrated core and operational Data: Gupta and Bhui. Natural Resources Research, 35(2), pp.1061-1093.

[7] Akhlaghi, M.A., Bagherpour, R. and Hoseinie, S.H., 2025. Real-time prediction of disc cutter wear in low-abrasive rocks: integrating physico-mechanical properties and signal processing features through machine learning methods. Arabian Journal for Science and Engineering, 50(16), pp.12513-12537.

[8] Maluventhi, S.K., Kulandaisamy, P., Rajendran, M., Balagurumoorthi, D.R. and Veeramalai, G., 2025. Machine learning-powered geospatial mapping of groundwater quality and salinity: towards sustainable water management in Southern India. Stochastic Environmental Research and Risk Assessment, 39(11), pp.5131-5150.

[9] Zhao, H., Ma, X., Fan, Y., Dong, X., Kang, Y. and Wen, P., 2025. Research on identification, separation and mechanism of soft and hard gangue from raw coal gangue via dual-energy X-ray based on machine learning. International Journal of Coal Preparation and Utilization, pp.1-22.

[10] Peng, T., Sun, T., Li, Y., Wang, B. and Zhang, J., 2025. Correlation between scratch hardness and plastic parameters of metallic materials: A comparative study of machine learning and empirical solution. Journal of Materials Research, 40(4), pp.572-584.

[11] Banu, S.A., Zhang, X., Mahgoub, S.A., Abedi, S. and Noshadravan, A., 2025, June. Machine Learning-Driven Micromechanical Characterization of Shale Rocks Leveraging High-Speed Nanoindentation Data. In ARMA US Rock Mechanics/Geomechanics Symposium (p. D021S013R003). ARMA.

[12] Ghadernejad, S. and Esmaeili, K., 2024. Predicting rock hardness and abrasivity using hyperspectral imaging data and random forest regressor model. Remote Sensing, 16(20), p.3778.

[13] Houshmand, N., Esmaeili, K., Goodfellow, S. and Ordonez-Calderon, J.C., 2023. Predicting rock hardness using Gaussian weighted moving average filter on borehole data and machine learning. Minerals Engineering, 204, p.108448.

[14] Liu, S., Zhao, H., Yuan, Z., Xiao, L., Shen, C., Wan, X., Tang, X. and Zhang, L., 2024. A Machine Learning Approach for the Autonomous Identification of Hardness in Extraterrestrial Rocks from Digital Images. Aerospace, 12(1), p.26.

[15] Gürkan, O.M., Gürkan, C., Baştürkcü, E., Timur, S.İ. and Yüce, A.E., 2026. A geometallurgical approach to hardness-controlled liberation and pre-concentration of critical minerals: barite-fluorite-REE. Canadian Metallurgical Quarterly, pp.1-19.

[16] Hadimani, L.A. and Vanarotti, M.B., 2026, March. Predicting Mohs Hardness of Minerals Using Neural Network Regression: A Machine Learning Approach. In 2026 International Conference on Machine Learning and Autonomous Systems (ICMLAS) (pp. 47-52). IEEE.

[17] Guo, Y., Zhang, W., Li, P., Zhao, Y., Mu, Z. and Yang, Z., 2025. Machine Learning-Enhanced Nanoindentation for Characterizing Micromechanical Properties and Mineral Control Mechanisms of Conglomerate. Applied Sciences, 15(17), p.9541.

[18] Cornu, P., Kane, M., Duc, M., Ropert, C., Lansac, F. and Gennesseaux, M., 2024. Long-term pavement friction: Improving the aggregate hardness parameters definition. Construction and Building Materials, 451, p.138924.

[19] Sharifi Teshnizi, E., Ghafoori, M., Lashkaripour, G.R., Khademi Hamidi, J. and Yousefi, A.H., 2026. Assessment and Prediction of Rock Drillability in Hard Granitic Rocks Using Experimental Testing and Machine Learning Models. Geopersia.

[20] Pinheiro, J.M.H., de Oliveira, S.V.B., Silva, T.H.S., Saraiva, P.A.R., de Souza, E.F., Godoy, R.V., Ambrosio, L.A. and Becker, M., 2025. The impact of feature scaling in machine learning: Effects on regression and classification tasks. IEEE Access, 13, pp.199903-199931.

[21] Chen, Y. and Hu, C., 2024. Hourly PM2. 5 concentration prediction based on empirical mode decomposition and geographically weighted neural network. *ISPRS International Journal of Geo-Information*, *13*(3), p.79.

[22] Amoako, P.Y.O., Cao, G., Shi, B., Yang, D. and Acka, B.B., 2025. Orthogonal capsule network with meta-reinforcement learning for small sample hyperspectral image classification. *Remote Sensing*, *17*(2), p.215.

[23] Gaspar, D., Silva, P. and Silva, C., 2024. Explainable AI for intrusion detection systems: LIME and SHAP applicability on multi-layer perceptron. IEEE Access, 12, pp.30164-30175.

[24] Zhou, Y., Huang, K., Cheng, C., Wang, X., Hussain, A. and Liu, X., 2022. FastAdaBelief: Improving convergence rate for belief-based adaptive optimizers by exploiting strong convexity. IEEE Transactions on Neural Networks and Learning Systems, 34(9), pp.6515-6529.

[25] https://www.kaggle.com/datasets/vinven7/comprehensive-database-of-minerals/data

[26] Hussain, J., Fu, X., Chen, J., Ali, N., Hussain, J., Hussain, S. and Ali, S., 2025. Advanced Hybrid Machine Learning Models Combined with Petrographic Analysis for Comprehensive Durability Assessment of Rock Construction Materials. *Intelligent Geoengineering.*

[27] Wang, L., Chen, H., Wang, B., Li, Q., Luo, Q. and Han, Y., 2024. Deep Learning-Driven Microstructure Characterization and Vickers Hardness Prediction of Mg-Gd Alloys. *arXiv preprint arXiv:2410.20402.*